Strain-sensing system based on carrier-modulated gratings for the monitoring of a large number of channels

Author/Contributor:
Childs, Paul; Wong, Allan; Peng, Gang-Ding

Publication details:
Journal of Lightwave Technology
v. 24
Chapter No. 3
pp. 1388-1394
0733-8724 (ISSN)

Publication Date:
2006

Publisher DOI:
http://dx.doi.org/10.1109/JLT.2005.863323

Strain-Sensing System Based on Carrier-Modulated Gratings for the Monitoring of a Large Number of Channels

Paul Childs, Allan C. L. Wong, and Gang Ding Peng

***Abstract*—The performance of a strain sensor system based on the use of carrier-modulated gratings and Fourier-domain decoding is analyzed. For three sensors, Young's modulus is measured as 69.98 $\pm$ 0.27, 69.15 $\pm$ 0.81, and 70.65 $\pm$ 0.58 GPa. Crosstalk is shown to exist only when two sensors are designed with an overlap of the carrier band in the Fourier domain. Improving the data processing shows it is possible to limit this crosstalk to a value below that of the system error.**

***Index Terms*—Gratings, harmonic analysis, optical fiber sensors, strain sensor.**

I. Introduction

IN QUASI-DISTRIBUTED fiber-optic strain-sensing systems, fiber Bragg grating (FBG)-based sensors are a definite candidate for use in smart materials and structures, and structural health monitoring (SHM) of large-scale structures such as bridges. The main issue is to implement a large number of sensors for such structures, so that it can provide adequate information for reliable and accurate SHM. There are a number of techniques to multiplex the sensing elements; the more common ones are time-division multiplexing (TDM), wavelength-division multiplexing (WDM), and spatial-frequency-division multiplexing.

TDM is a mature and widely used technique in telecommunications, but it requires accurate switching, long delay lines, and suffers from poor signal-to-noise ratio (SNR) of sensed signals. WDM is a natural choice because of the wavelength-encoded nature of FBG. However, most FBG sensors employ amplified spontaneous emission (ASE) using an erbium-doped fiber amplifier (EDFA) as the light source, which is bandlimited to about 50 nm for good SNR. Thus, the maximum number of sensors that can be multiplexed is limited to about eight channels for measuring strains of up to 5000 $\mu\varepsilon$. Spatial-frequency-division multiplexing makes use of Fourier transform to obtain the spatial frequency and phase information from the sensed signals. For example, in the fiber Fizeau strain sensor system [1], each sensor has a different cavity length. By Fourier transforming the multiplexed signals, each sensor corresponds to a distinct peak (related to its optical path difference) in the Fourier magnitude spectrum, provided cavity-length separation for each sensor is sufficiently large. However, the system is incompatible with WDM, and the upper limit to the number of channels due to fringe visibility decreasing with the cavity length is still insufficient.

Other techniques, such as the use of genetic algorithms [2] to converge to a solution for the strain of each sensor even when the spectrum overlaps, have been proposed but require long processing times, making them unsuitable for use in real-time-monitoring systems.

A multiplexing technique utilizing both WDM and harmonic division multiplexing (W*DM) has been proposed [3], and preliminary experimental results of a proof of principle have been shown [4]. This technique overcomes the incompatibility of the Fizeau sensor with WDM by using carrier-modulated gratings that have a narrow bandwidth in both the wavelength and Fourier domains. As it makes use of fast Fourier transforms, which are processed in the order of milliseconds, the system is compatible with real-time monitoring.

II. Theory

The process of obtaining the strain of various sensors $\varepsilon_{k,j}$ from a given reflection spectrum R is represented mathematically by a chain of operators $\varepsilon \circ \overline{d\Phi} \circ M_j \circ X \circ S_k \circ \mathrm{Adc}_m \circ P \circ F \circ R$, each of which is detailed in [3]. Here, R represents the return optical signal from the sensor array. F represents the effect of passing through a fiber Fabry–Pérot interferometer (FFPI) or other such spectrally selective device. P represents the conversion from an optical signal to an electrical signal by a photodiode. Adc_m represents the mth data set collected by an analog to digital card. S_k represents the data set corresponding to the kth WDM channel. X represents a correction-factor operator. M_j represents the data set corresponding to the jth W*DM channel of the Fourier-transformed data set. $\overline{d\Phi}$ represents a weighted-averaged differential phase operator, and ε represents the operator for evaluating the resultant strain.

The reflection spectrum of the gratings used in such a scheme is defined in (1), shown at the bottom of the next page.

A grating fabricated according to this equation with $j = 2$ is shown in Fig. 1.

Manuscript received March 13, 2005; revised October 21,2005. This work was supported in part by the Australian Research Council and the Roads and Traffic Authority of Australia.

The authors are with the School of Electrical Engineering, University of New South Wales, Sydney 2052, Australia (e-mail: p.childs@student.unsw.edu.au; allanw@student.unsw.edu.au; g.peng@unsw.edu.au).

Digital Object Identifier 10.1109/JLT.2005.863323

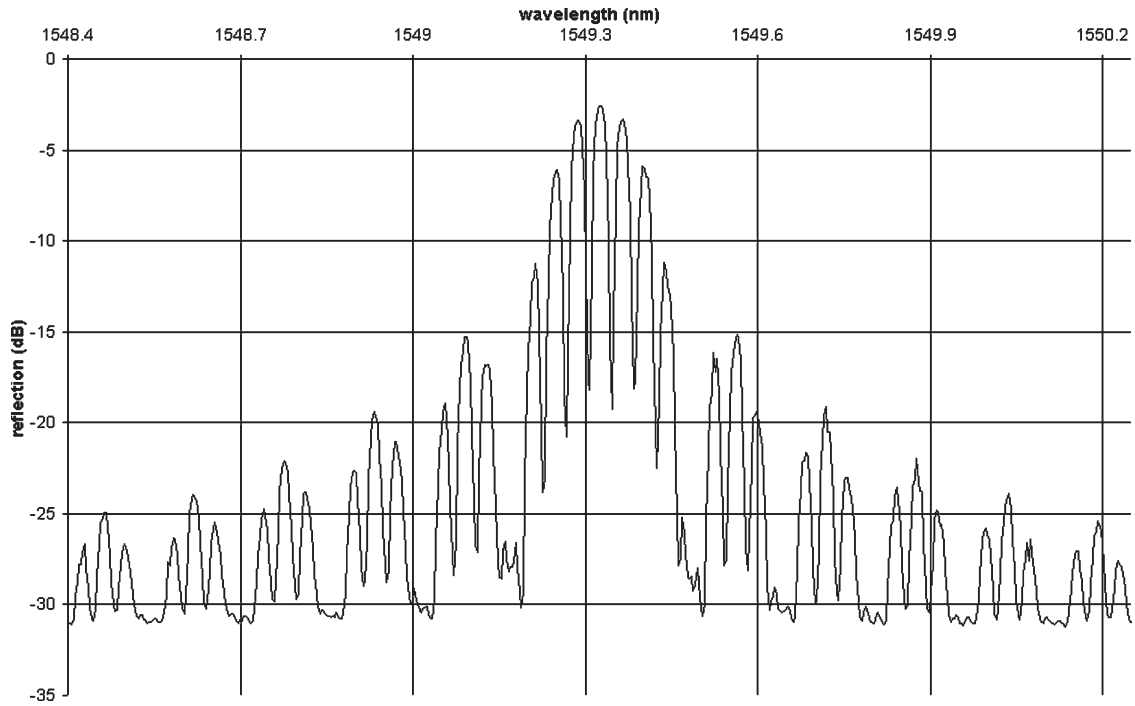

Fig. 1. Measured spectrum of the $j = 2$ grating.

For the purpose of testing the system, we interrogated the gratings using a C-band tuneable laser, rather than an FFPI. As such, the linewidth of the tuneable laser can be assumed to be negligible with respect to the sampling resolution. The laser is scanned with a linear sweep rate of 3 nm/s from 1520 to 1570 nm and measured at a sampling density of $\rho = 278$ points/nm. Reference measurements are taken to compensate for the responsivity of the detector and the source strength of the laser (i.e., effectively, $D(\lambda) = A(\lambda) = 1$). Thus, the operators PF given in [3] reduce to

$$\begin{aligned} P \circ F(t) &= \int_{-\infty}^{\infty} D(\lambda) R(\lambda) \text{FFPI}\left(\lambda - \lambda_{\text{FFPI}}(t \bmod \tau)\right) d\lambda \\ &= \int_{-\infty}^{\infty} R(\lambda) \delta(\lambda - 1520 - 3t \bmod 50) d\lambda \\ &= R(1520 + 3t \bmod 50). \end{aligned}$$

Furthermore, the correction-factor operator simplifies to

$$X_{\kappa,m}(x) = \chi_{I_2}(x) \phi\left(S_{\kappa,m}\{x\}\right)$$

where $\phi(\bullet) = \log_2(1 - \bullet)$, and $\chi_I(x)$ is the characteristic function on the interval I, i.e., it is equal to 1 when x is an element of I and 0 otherwise. Thus, the need for two of the three Fourier transforms per scan, which are associated with the deconvolution of the FFPI operator, is eliminated.

Spectral shadowing is an effect that occurs in multiplexed systems when a downstream grating will receive less power than an upstream grating due to the upstream grating shadowing out a portion of the spectrum of the source. This effect is enhanced when the gratings used have a high reflectivity. The introduction of spectral shadowing changes the system from a linear one to a nonlinear one, and for this reason, $R_{k,j}(\lambda)$ has an exponential term, and $\phi(\bullet)$ is required to relinearize the system response.

The remaining operators not given so far are given in the equations shown at the bottom of the next page, where $\Delta = \Gamma \varepsilon_{\max} \lambda_0 \rho$ and $\Gamma = 0.78$.

The weighting function $w(s)$ was taken to be a triangular hat function covering I_3. As only one WDM channel is tested, the size of the buffer region between WDM channels ξ is taken to be 0. The constant o, which is used to eliminate the ringing when performing deconvolution, is also unnecessary and can be taken to be 0 as well. This resulted in $I_1 = I_2 = (0, \Delta)$. I_3 was determined semi-empirically from the measured Fourier spectrum.

Applying a stress of τ_a to grating a and τ_b to grating b, the interplay between the two gratings of a strain signal crossing from grating a to grating b can be modeled by assuming that

$$R_{k,\mathrm{j}}(\lambda) = 1 - 10^{\frac{-L_{k,\mathrm{j}}}{10}} \cos^2 \frac{(j+\eta)\pi\left(\rho(\lambda - \lambda_{0,k})\right)}{2n+1} \operatorname{sinc}^2 \frac{(1-\zeta)\left(\rho(\lambda - \lambda_{0,k})\right)}{4n+2} \tag{1}$$

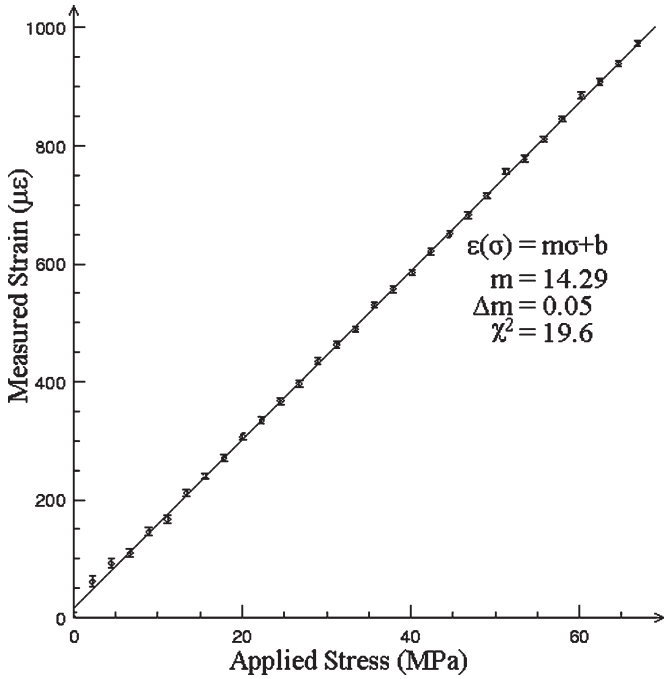

Fig. 2. Stress–strain relation for the $j = 1$ channel.

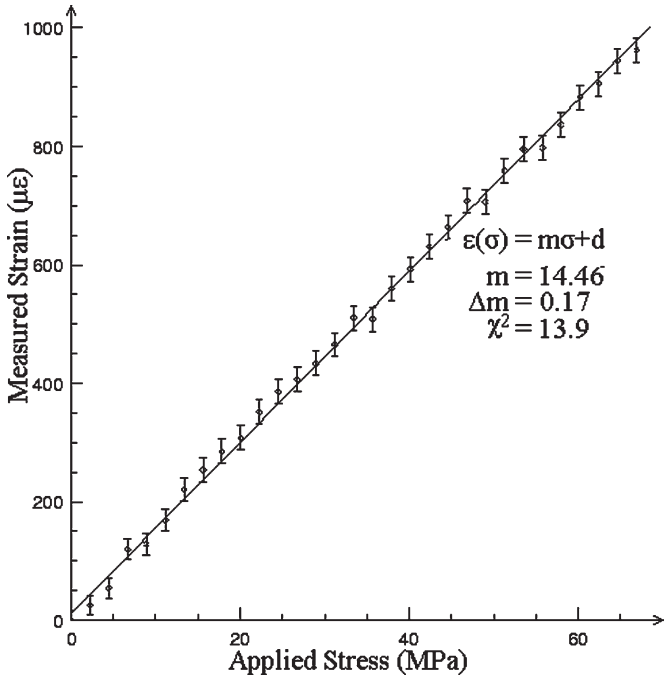

Fig. 3. Stress–strain relation for the $j = 2$ channel.

the strain response of grating b is due to the sum of a linearly correlated part and an uncorrelated part, i.e.,

$$b = aX_{a\to b} + v : \sum_{\tau_a} [v - \langle v\rangle_a]\,[a - \langle a\rangle_a] = 0$$

where $\langle\omega\rangle_a$ denotes the mean of ω taken with respect to τ_a. The cross correlation coefficient $X_{a\to b}$ can be found as

$$X_{a\to b} = \frac{\sum_{\tau_a}[b - \langle b\rangle_a]\,[a - \langle a\rangle_a]}{\sum_{\tau_a}[a - \langle a\rangle_a]^2}. \tag{2}$$

The error associated with measuring this factor is fairly complicated due to the error in a and b being dependent on the configuration state of the entire system, e.g., the error associated with measuring the strain for a and b is greater when they overlap either each other or another grating. Given errors da and db, which are functions of τ_a and τ_b, the error in the correlation coefficient is

$$dX_{a\to b} = \frac{\sum_{\tau_a}[b - \langle b\rangle_a - 2X_{a\to b}(a - \langle a\rangle_a)]da + [a - \langle a\rangle_a]db}{\sum_{\tau_a}[a - \langle a\rangle_a]^2}.$$

III. Experiment

Three gratings corresponding to $\{j\} = \{1, 2, 2.5\}$, a center wavelength of 1550 nm, and an insertion loss of $\sim$ 3.5 dB were fabricated by Redfern Optical Components according to the specifications given in (1). The gratings were then spliced together in a series architecture with the ordering {2.5, 1, 2}; the former being the closest to the light source. However, the

$$R(\lambda) = 1 - \prod_{k,\mathrm{j}} (1 - R_{k,\mathrm{j}}(\lambda))$$

$$\mathrm{Adc}_m(x) = \chi_{(1520\rho,1570\rho)}(x) P\left(50m + \frac{1}{3}\left(\frac{x}{\rho} - 1520\right)\right)$$

$$S_\kappa(x) = \chi_{I_1}(x)\mathrm{Adc}(\rho\lambda_{0,\kappa} + x - \xi - o)$$

$$M_\gamma^+(s) = \chi_{I_3}(s)\mathcal{F}\left(X(x)\right)$$

$$\overline{d\Phi} = \frac{\sum\limits_s w(s)\left(\tan^{-1}\left(\frac{\mathrm{Re}(M(s))}{\mathrm{Im}(M(s))}\right) - \tan^{-1}\left(\frac{\mathrm{Re}\left(M\left(s+\frac{1}{\Delta}\right)\right)}{\mathrm{Im}\left(M\left(s+\frac{1}{\Delta}\right)\right)}\right)\right)}{\sum\limits_s w(s)}$$

$$\varepsilon = \frac{1}{\rho\Gamma\lambda_0}\left(\frac{\Delta\overline{d\Phi}}{2\pi} - \xi - o\right)$$

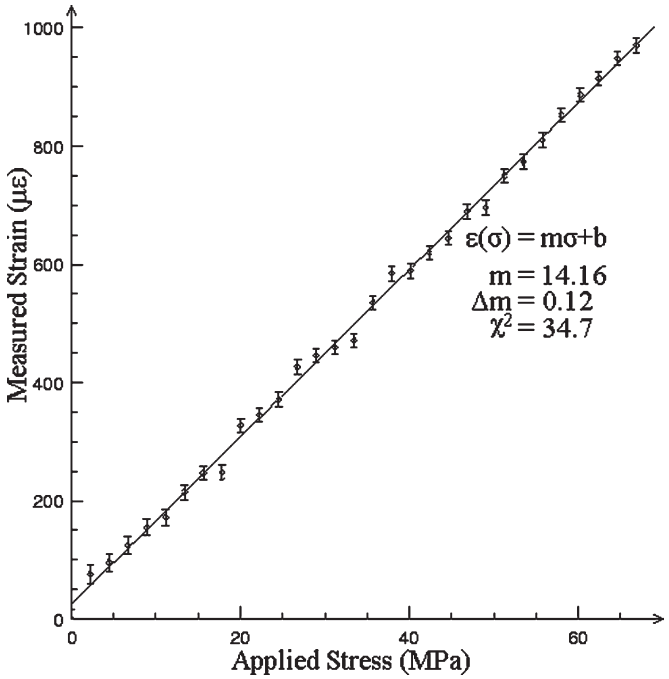

Fig. 4. Stress–strain relation for the $j = 2.5$ channel.

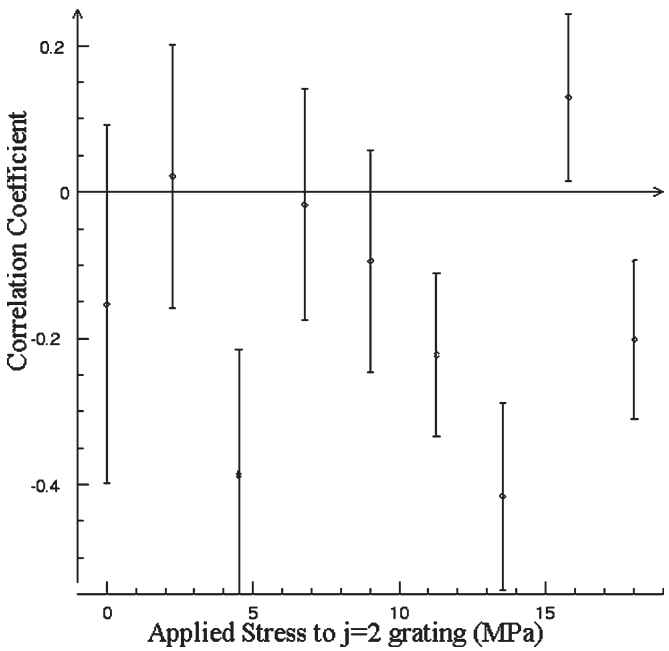

Fig. 5. Cross-correlation coefficient from $j = 1$ to $j = 2$.

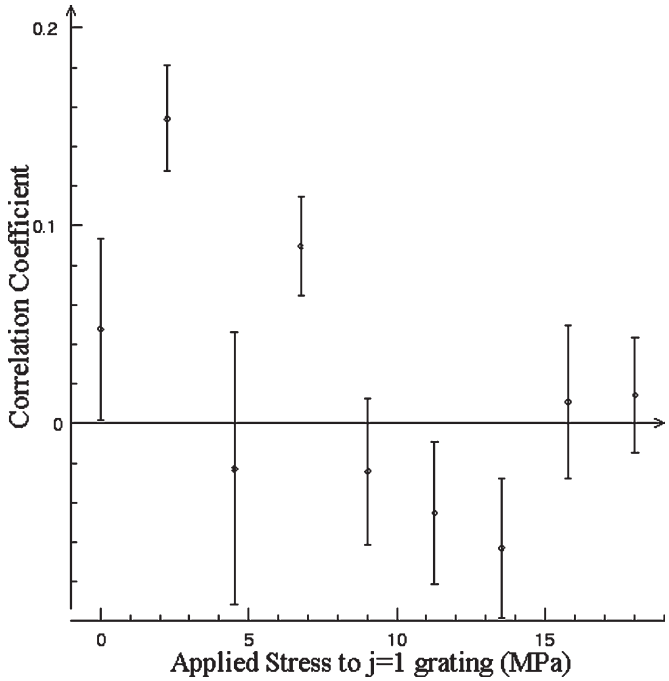

Fig. 6. Cross-correlation coefficient from $j = 2$ to $j = 1$.

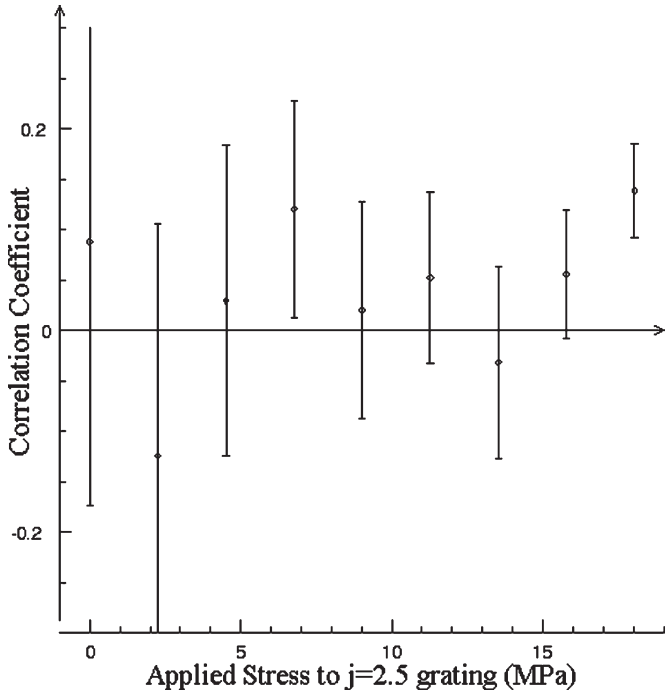

Fig. 7. Cross-correlation coefficient from $j = 2$ to $j = 2.5$.

ordering was not considered important as the formula for the reflection spectrum was seen to be invariant under interchanging of the gratings. Short lengths of cotton were threaded through the splice protectors prior to heating to enable weights to be attached. The gratings were loaded vertically with a 20-cent coin (11.2 g) to provide enough weight to give stability. This was considered to be the zero-strain condition. Interrogation of the three gratings was carried out using a C-band tuneable laser and a 3-dB coupler to measure the reflected spectrum.

Loading trials were performed by varying the load applied to one of the gratings while the other two remained at the zero-strain condition. The tests were performed for each of the gratings being the load bearer. Five-cent coins (2.8 g) were used as the weights for applying strain to the gratings.

Crosstalk trials were performed by varying the load applied to one of the gratings while one of the other gratings was at a fixed strain state, and the third was kept at the zero-strain condition. The strain of the varying channel and the fixed state channel was measured. The strain values applied were limited to a small range where the spectrum of all the gratings would be most strongly overlapping. This was done to characterize

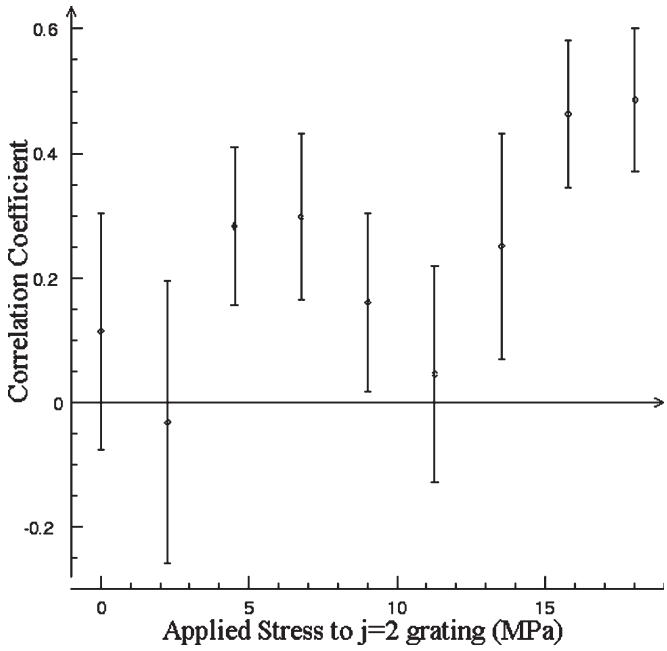

Fig. 8. Cross-correlation coefficient from $j = 2.5$ to $j = 2$.

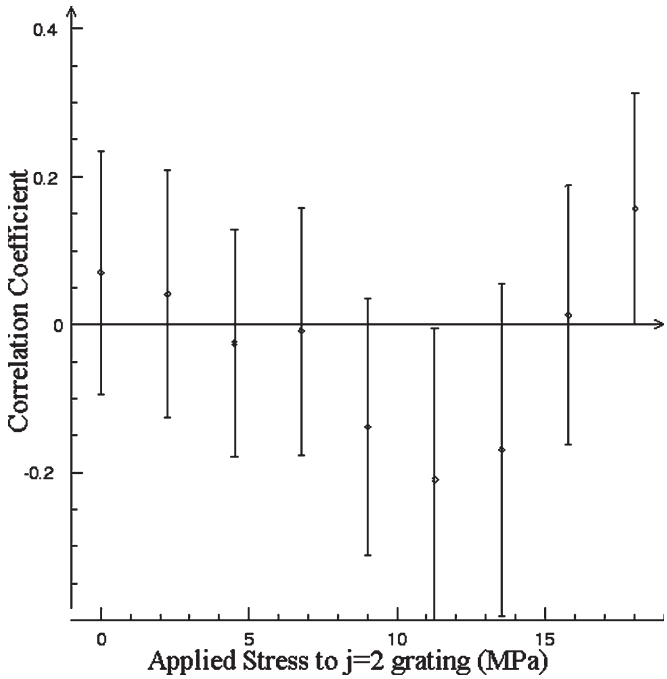

Fig. 9. Cross-correlation coefficient from $j = 2.5$ to $j = 2$ with narrower windowing in W*.

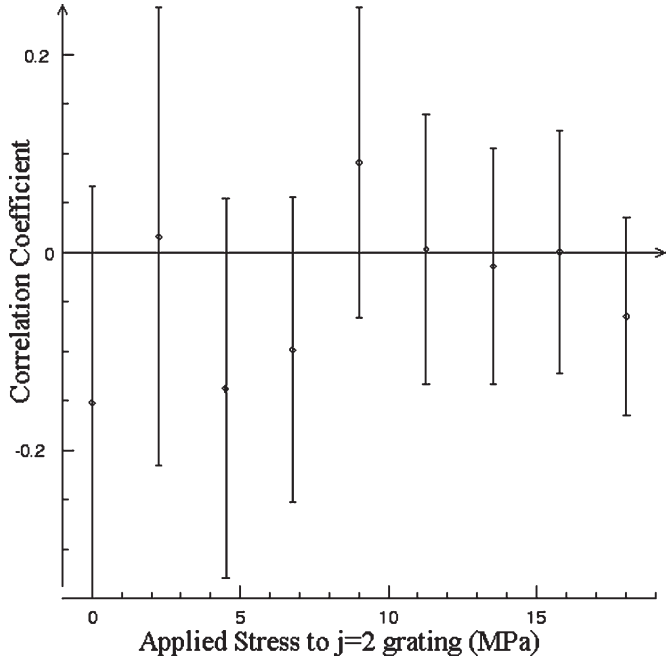

Fig. 10. Cross-correlation coefficient from $j = 1$ to $j = 2$ with narrower windowing in W*.

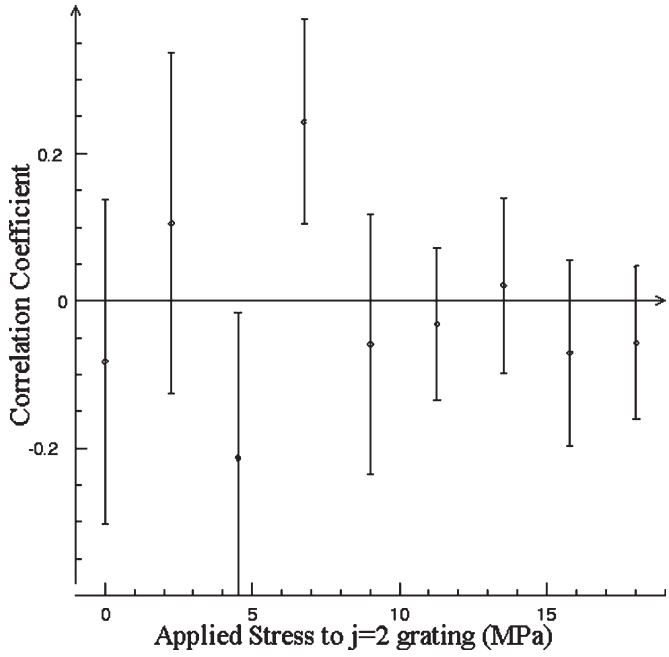

Fig. 11. Cross-correlation coefficient from $j = 1$ to $j = 2$ with narrower windowing in W* and without spectral-shadowing compensation.

the worst-case scenario with respect to crosstalk. Resultant correlation coefficients were obtained using (2) for each strain value of the fixed strain-state grating. The tests were repeated so as to determine $X_{1\to2}$, $X_{2\to1}$, $X_{2\to2.5}$, and $X_{2.5\to2}$. To gain a better understanding of the crosstalk, all of these results were processed according to three cases: 1) standard processing; 2) narrower windowing of data in W*; and 3) narrower windowing of data in W* and removal of the correction algorithm for spectral shadowing.

In order to evaluate the error associated with each of the above measurements, various loading configurations were selected, and 25 measurements of the strain of all channels were performed for each configuration over the same time frame as that of the above tests. The standard deviation was taken and the resultant configurational error lattice interpolated to give an error value for each strain state measured in the above tests.

The results of the loading tests for the cases of grating $j = 1$, 2 and 2.5 being the grating under test are plotted in Figs. 2–4, respectively. The correlation coefficient $X_{a\to b}$ as a function of

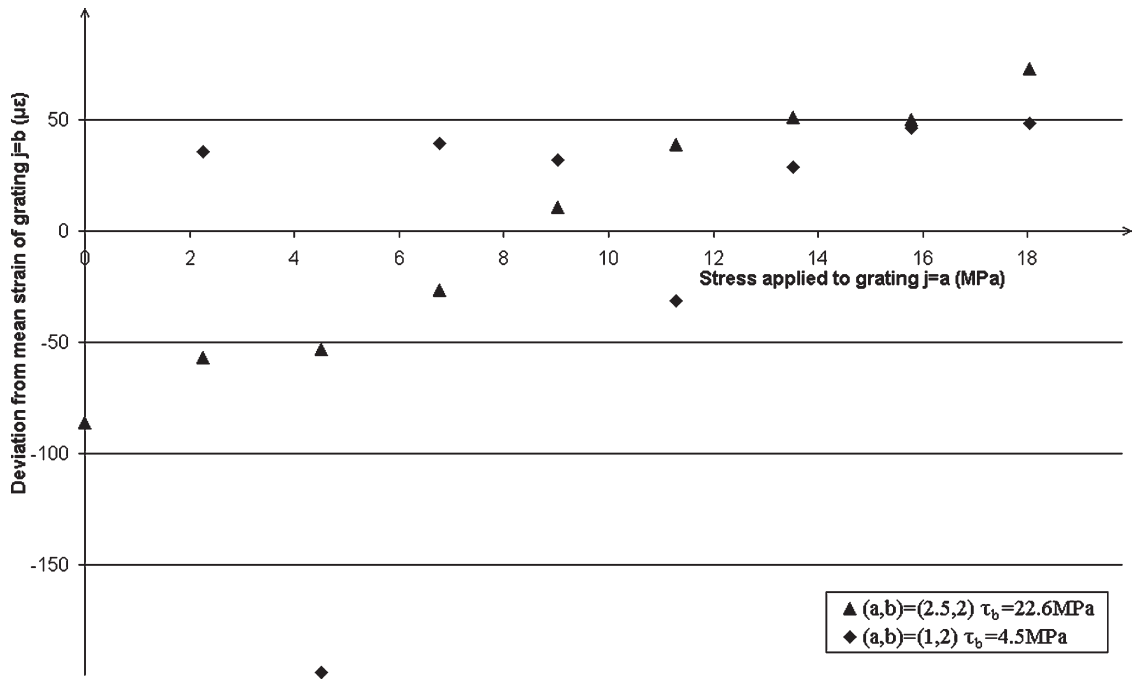

Fig. 12. Trends in the b channel when calculating $X_{a\to b}$ for the two cases given in the legend.

the strain state τ_b is plotted in Figs. 5–8 for the cases of $(a, b) = (1, 2)$, $(2, 1)$, $(2, 2.5)$, and $(2.5, 2)$, respectively. Fig. 9 shows $X_{2.5\to 2}$ using narrower windows in W* to process the data in an attempt to reduce the crosstalk. Figs. 10 and 11 show $X_{1\to 2}$ with and without the use of the correction algorithm for spectral shadowing; both using narrower windows in W* for the data processing.

IV. Analysis

The values of Young's modulus for the fibers based on the loading tests on fibers $j = 1$, 2, and 2.5 were calculated as 69.98 $\pm$ 0.27, 69.15 $\pm$ 0.81, and 70.65 $\pm$ 0.58 GPa, respectively. These were found to be in good keeping with the theoretical value of 70.3 GPa for fused silica.

In examining the crosstalk between the gratings, it must be remembered that we are looking at a very small effect, and as such, it is difficult to distinguish from the error involved with making measurements. Furthermore, the error did not seem to follow a normal distribution (i.e., for larger errors, the probability of error did not drop off as rapidly as x^{-2}), making the standard deviation (a second-order moment) not the best indicator of the expected amount of error. Where this was the case, a lower order moment was chosen to more accurately characterize the measurement error for the purpose of the error calculations.

Nevertheless, the results showed a clear distinction between the three cases of $X_{1\to 2}$, $X_{2\to 1}$, and $X_{2\to 2.5}$ compared with that of $X_{2.5\to 2}$. For the case of the former three, in the main part, any possible crosstalk was within error of being 0, whereas that of the latter case showed a clear positively correlated monodirectional crosstalk from grating $j = 2.5$ to grating $j = 2$. There were a few cases where this was seen not to be the case (particularly, some of those for $X_{1\to 2}$), but the most prominent of these cases show that they are dominated by one or more of the spurious readings associated with the abovementioned deviations from the normal distribution (an example of which is shown in Fig. 12). Except for the measurement of 6.8 MPa of stress applied to grating $j = 2$, the measurements of $X_{2.5\to 2}$ showed a clear trend across $\tau_{2.5}$, giving rise to the calculated value of the correlation coefficient (an example of which is also found in Fig. 12). Averaging over all the measured configurations gave $\langle X_{2.5\to 2}\rangle_b = 0.23$.

For the case of using a smaller range of data in W* for the processing, the range used was slightly less than half of the full-width range. This allowed for the windows from the $j = 2$ and $j = 2.5$ gratings to be nonoverlapping, though there was still an encroaching of spectra from each grating into the window of the other. In this case, all of the calculated values of the correlation coefficient came within error of equalling 0. This was most evident for the case of $X_{2.5\to 2}$. This confirmed the idea that the origin of the crosstalk was from a mixing of the signals due to overlapping of spectra in the Fourier domain. It also showed that if the channel count was a crucial issue, it would be possible to more densely multiplex the sensors beyond the traditional $j = 1 + n$ (where n is a natural number) to $j = 1 + n/\varepsilon$, such that $1 \le \varepsilon \le 2$ by using a smaller data range in W* to limit the crosstalk down to a manageable value.

The use of, or removal of, correction for spectral shadowing, i.e., the operator $\phi(\bullet)$, had little effect on the final results. There was found to be more anomalous errors generated when the spectral-shadowing algorithm was removed. The rms values of the correlation coefficients changed from 0.08, 0.05, 0.05, and 0.12 to 0.12, 0.07, 0.08, and 0.11 with the removal of the correction for spectral shadowing. As each of the gratings had a low reflectivity ($\sim$ 3.5 dB), the effect of spectral shadowing

was not a crucial one, even when the gratings were completely overlapped. This would change, however, if more sensors were to be multiplexed within the one WDM window.

V. Conclusion

The proof of the principle of using carrier-modulated gratings and harmonic analysis to decode the strain of each sensor was demonstrated in the successful measurement of the strain of three strongly overlapping gratings. The measured values of the strain closely followed the actual values, which was seen in the determination of Young's modulus of the fibers as 69.98 $\pm$ 0.27, 69.15 $\pm$ 0.81, and 70.65 $\pm$ 0.58 GPa, compared with the theoretical value of 70.3 GPa. An analysis of the crosstalk involved in the system showed that between two gratings that were nonoverlapping in the Fourier domain, the worst-case scenario resulted in a value for the crosstalk that was within measurement error of being 0. Crosstalk was shown to exist for the case of two gratings that were overlapping in the Fourier domain; however, it was shown that this could be reduced to a manageable value by improving the processing techniques by tightening the windowing in the Fourier domain to a region where the degree of overlap is smaller.

Acknowledgment

The authors would like to thank A. Buryak and G. Edvell for formulating an inverse scattering solution and the fabrication of the required gratings.

References

[1] Y. J. Rao, J. Jiang, and C. X. Zhou, "Spatial-frequency multiplexed fiber-optic Fizeau strain sensor system with optical amplification," *Sens. Actuators A, Phys.*, vol. 120, no. 2, pp. 354–359, May 2005.

[2] C. Z. Shi, C. C. Chan, W. J. Jin, Y. B. Liao, Y. Zhou, and M. S. Demokan, "Improving the performance of a FBG sensor network using a genetic algorithm," *Sens. Actuators A, Phys.*, vol. 107, no. 1, pp. 57–61, Oct. 2003.

[3] P. Childs, "An FBG sensing system utilizing both WDM and a novel harmonic division scheme," *J. Lightw. Technol.*, vol. 23, no. 1, pp. 348–354, Jan. 2005.

[4] P. Childs, T. Whitbread, and G.-D. Peng, "Spectrally-coded multiplexing in a strain sensor system based on carrier-modulated fiber Bragg gratings," in *Proc. SPIE*, Beijing, China, 2005, vol. 5634, pp. 204–210.

Paul Childs was born in New South Wales, Sydney, Australia, in 1980. He received the B.Sc. degree in physics in 2000 and the M.Sc.Tech. degree in photonics in 2002 from the University of New South Wales, where he is currently working toward the Ph.D. degree in electrical engineering.

He worked in the fields of fiber-grating fabrication and fiber characterization at JDS Uniphase, Sydney, from mid-2000 to mid-2002.

Allan C. L. Wong was born in Hong Kong. He received the B.Sc. degree in physics from Flinders University, Adelaide, Australia, in 1998. In 2002, he received the B.Sc. (Hons.) degree in physics from University of Adelaide, Adelaide, Australia, where he is currently working toward the M.Sc. (research) degree in physics. Currently, he is working toward the Ph.D. degree in electrical engineering at the University of New South Wales, Sydney, Australia.

From 1998 to 2000, he worked as a Computer Programmer in Hong Kong.

Gang Ding Peng received the B.Sc. degree in physics from Fudan University, Fudan, China, in 1982 and the M.Sc. degree in applied physics and the Ph.D. degree in electronic engineering, both from Shanghai Jiao Tong University, Shanghai, China, in 1984 and 1987, respectively.

From 1987 to 1988, he was on the Faculty of Jiao Tong University. He was in the Optical Sciences Centre of the Australian National University, Canberra, Australia, from 1988 to 1991. He is presently an Associate Professor with the School of Electrical Engineering and Telecommunications, University of New South Wales, Sydney, Australia. His research interests include optical fiber and waveguide devices, polymer optical fibers, optical fiber sensing, and nonlinear optics.

Dr. Peng was a Queen Elizabeth II Fellow from 1992 to 1996.